Journal of Power Sources xxx (xxxx) xxx

Contents lists available at ScienceDirect

Journal of Power Sources

journal homepage: www.elsevier.com/locate/jpowsour

Exploring the thermodynamics of the bromine electrode in concentrated solutions for improved parametrisation of hydrogen–bromine flow battery models

Jakub K. Wlodarczyk [a,*], Michael Küttinger [b], Andreas K. Friedrich [c], Jürgen O. Schumacher [a]

[a] Institute of Computational Physics, Zurich University of Applied Sciences, Wildbachstrasse 21, 8401 Winterthur, Switzerland
[b] Fraunhofer Institute for Chemical Technology, Joseph-von-Fraunhofer-Strasse 7, 76327 Pfinztal, Germany
[c] German Aerospace Center, Institute of Engineering Thermodynamics, Electrochemical Energy Technology, Pfaffenwaldring 38-40, 70569 Stuttgart, Germany

HIGHLIGHTS

- A novel thermodynamic bromine electrode model is described and validated.
- It is applied to describe the open-circuit voltage of a pilot-scale flow battery.
- Polybromide formation constants are re-evaluated at high electrolyte concentrations.
- Mean activity coefficient of aqueous HBr up to 11 m between 0 and 70 °C is modelled.

GRAPHICAL ABSTRACT

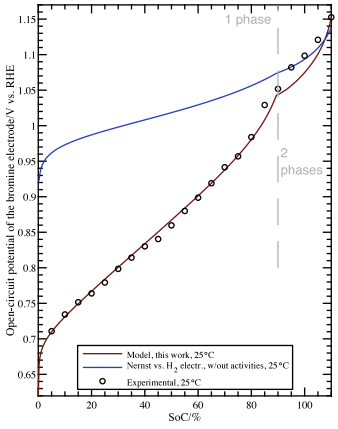

ARTICLE INFO

Keywords:
Thermodynamics
Modelling and simulation
hydrogen–bromine redox flow battery
Open circuit potential
Bromine electrode
Activity coefficient

ABSTRACT

Thermodynamic properties of the bromine electrode in an exemplary hydrogen–bromine flow battery (HBFB) are investigated in detail. Open-circuit potential (OCP) measurements of HBRB electrolytes in a liquid junction-free setup and electrolyte Raman spectra are employed to estimate polybromides speciation. An improved mathematical description of the bromine electrode OCP versus state of charge is provided.

This paper addresses the phenomenon of polybromides formation at concentrations up to 7.7 mol L^{-1} HBr and 3.85 mol L^{-1} Br_2 and their significant impact on the OCP. The model takes into account tri-, penta- and heptabromides formation, precisely modelled electrolyte activity coefficients (up to 11-molal HBr), electrolyte density, and temperature. It is elucidated that the polybromide formation constants found in literature treating dilute electrolytes are substantially too low. Newly determined equilibrium constants, applicable over a wider concentration range are provided for 25 and 43 °C together with their standard enthalpy changes. The model is successfully validated in an independent experiment using a real, pilot-scale HBFB.

It is concluded that the usage of a simple Nernst-like equation to calculate the OCP of flow battery electrodes containing concentrated electrolytes leads to erroneous results.

* Corresponding author.
E-mail addresses: jakub.wlodarczyk@zhaw.ch (J.K. Wlodarczyk), michael.kuettinger@gmx.de (M. Küttinger), andreas.friedrich@dlr.de (A.K. Friedrich), juergen.schumacher@zhaw.ch (J.O. Schumacher).

https://doi.org/10.1016/j.jpowsour.2021.230202
Received 19 October 2020; Received in revised form 20 May 2021; Accepted 20 June 2021

1. Introduction

An economically viable redox flow battery (RFB) system is characterised by low cost of energy storage, which can be achieved by increasing the battery energy density (e.g. augmenting electrolyte concentrations) [1,2]. High concentrations imply complications in the thermodynamic description of the electrolytes found in RFB and pose problems in parametrisation of numerical RFB models [3]. In one of the early papers analysing the performance of a hydrogen–bromine flow battery (HBFB) cell [4], the authors used a complicated empirical expression in order to model the cell voltage. In a modern paper by Ronen et al. [5], the HBFB electrolyte was used as an example to derive a theory of a cell in which a fast homogeneous reaction, such as complex formation, takes place. It was pointed out that a presence of thermodynamic effects such as ionic equilibria influences also electrode kinetics and transport processes.

In this study, an attempt to quantify the thermodynamic phenomena occurring in highly concentrated bromine half cell electrolytes (posolytes in HBFB) is made in order to steer clear of using complex empirical formulae, formal potentials or fitting, and to increase versatility and predictivity of the HBFB or other bromine-based cell models. The goal of this paper is to (1) provide a framework for scrutinising thermodynamic phenomena occurring in real flow batteries employing the bromine electrode, especially the HBFB, (2) explain by means of a mathematical model the dramatic impact of these phenomena on the cell open-circuit voltage, OCV, (the versatile model was validated in a real HBFB pilot-scale system) (3) provide a tool for predicting bromine RFB electrode half-cell potential as a function of broad range of electrolyte compositions and temperatures (4) discuss the relevance of cell equilibrium thermodynamics as well as thermodynamics-related polarisation effects such as concentration polarisation for the practical operation of bromine-based (HBFB, V–Br, Zn–Br) and other halogen-based RFBs.

The paper is organised as follows. In Section 2, a review of the currently existing knowledge on the bromine electrolyte and known phenomena is presented. Next, a description of experimental studies performed to measure the open-circuit potential (OCP) of the bromine electrode and a model validation procedure in a real pilot-scale HBFB cell are given in Section 3. Section 4 contains an elaboration on the OCP model development and a method to calculate polybromides formation equilibrium constants. Sections 5 and 6 discuss the outcomes and conclusions of the current study and delineate possible directions of further model development. Companion supplementary material (SM) available online contains derivations and raw experimental data with experimental uncertainty calculations which did not fit into the volume of this research paper.

2. Thermodynamics in real hydrogen–bromine flow batteries

2.1. State of the art

Real HBFB and other bromine-based RFB systems, operate at much different conditions from those commonly encountered in electroanalytical chemistry. Higher electrolyte concentration up to 7–8 M HBr is dictated by energy density requirements and capital cost reductions [6–9]. During operation (especially charging process), HBFB stacks warm up significantly, which necessitates a separate heat exchange system. Cooling, in turn, entails extra power consumption, hence operating the battery at elevated temperatures up to 50 °C is a measure to mitigate the parasitic power losses. The presented departures from the standard conditions complicate the theoretical description of the real bromine electrode thermodynamic properties, which is indispensable for devising predictive models and simulations.

One of the most fundamental parameters strongly affected by thermodynamic phenomena is the cell OCP. The impact on the OCP or on the battery OCV was indicated for other common RFBs, e.g. the vanadium RFB [10]. Another study on vanadium systems [11] emphasised the importance of solution non-ideality as well as effects associated with charged ion-exchange membranes on the OCV. An extensive study on vanadium–hydrogen RFB [12] (page F1726) underlines the importance of correct elucidation of OCP-affecting issues as the key for the accuracy of model predictions and overpotential contributions estimations.

The equilibrium potential, $E_{\mathrm{eq},\mathrm{Br_2/Br^-}}$, of the Br_2(aq)/Br^- electrochemical half-cell couple (4) is defined by the Nernst equation (see also Appendix A in the SM):

$$E_{\mathrm{eq},\mathrm{Br_2/Br^-}} = E^{\circ}_{\mathrm{Br_2/Br^-}} + \frac{RT}{2F}\ln\left(\frac{a_{\mathrm{Br_2}}}{a^2_{\mathrm{Br^-}}}\right) \tag{1}$$

where $E^{\circ}_{\mathrm{Br_2/Br^-}}$ is the standard potential, T is the absolute temperature, R is the universal gas constant, F is the Faraday constant, and a is the activity of species.

The current literature treating modelling and simulation of bromine-based RFBs [13–15] does not pay particular attention to accurate modelling of cell thermodynamics dependence on species concentrations, e.g. the State of Charge (SoC) variation. Huskinson and Aziz [16] indicated the necessity of including molar activity coefficients, γ_i, of the redox species in modelling of HBFB, however they eventually either assumed $\gamma_i = 1$ or reverted to a semi-empirical expression from [4]. Savinell and Fritts [17] experimentally explored the applicability of the semi-empirical expression and the maximum relative error of ca. 6% was reported. A more recent study [5] briefly discusses the consequence of complexation phenomena on the electrode potential as well as the electrode kinetics in the bromine–bromide–water system.

In a recent paper by Duranti et al. [18], thermodynamic properties of the system Br_2-HBr-H_2O at higher concentrations (up to 2 M Br_2 and 4 M HBr) were examined experimentally in a setup without the elimination the liquid junction (LJ) and an OCV model was presented. This paper considered fitted parameters in different models of γ of HBr solutions and formation of tri- and pentabromine complexes.

2.2. Tri-, and pentabromide equilibria in aqueous solutions

The non-trivial properties of the bromine–bromide–water system were reported already in 1898 by Jakowkin [19]. A strong evidence in support of the existence of homogeneous bromine complexation reactions is based on the increased solubility of Br_2 in water when Br^- ions are present [20]. Despite the bromine dissociation in water described by reaction (D.1) in the SM, bromine is rather moderately soluble in water (0.2141 $\mathrm{mol\,L^{-1}}$ at 25 °C [21]). The polybromide formation can also be confirmed by means of modern analytical chemistry techniques such as Raman spectroscopy [7,22,23].

In bromide solutions richer in bromine, the increased solubility of bromine cannot be explained by the formation of Br_3^- alone, and therefore also Br_5^- is believed to exist [20,23–26]. By analysing a system of possible reactions [27], the dependent ones can be eliminated, so that the only independent reactions read:

$$\mathrm{Br_2 + Br^- \overset{K_3}{\rightleftharpoons} Br_3^-} \tag{2}$$

$$\mathrm{2Br_2 + Br^- \overset{K_5}{\rightleftharpoons} Br_5^-} \tag{3}$$

$$\mathrm{\frac{1}{2}Br_2 + e^- \rightleftharpoons Br^-} \tag{4}$$

Reactions (2) and (3) are homogeneous and reaction (4) is heterogeneous. All the mentioned species are assumed to be present in the form of an aqueous solution. Bromine hydrolysis can be neglected for the reasons described in Appendix D in the SM. An increase of K_5 with increasing ionic strength was reported by Jones and Baeckström [20] and this fact is of importance for the interpretation of the results later in this paper.

It is imperative to distinguish at this stage the stoichiometric (or apparent) equilibrium constant obtained from experiments (K'), frequently reported as dependent on the ionic strength of the solution, and the thermodynamic equilibrium constant (K), which is dependent only on temperature [28]. In some papers, the aforementioned K' were obtained at low ionic strengths (e.g. 0.2 M in HBr) which casts doubts on their applicability in more concentrated solutions (above 1 M), commonly utilised in RFB systems. By and large, reporting K' seems to be reasonable only together with ionic strengths (or a range thereof) in which the constant is applicable [28]. Table 1 juxtaposes literature values of equilibrium constants.

For the formation of the respective complex polybromide ions (reaction (2) and (3)), the following stoichiometric equilibrium constants are defined:

$$K'_3 = \frac{c_{Br_3^-}/c^\circ}{c^F_{Br_2} c^F_{Br^-}/c^{\circ 2}} \quad (5)$$

$$K'_5 = \frac{c_{Br_5^-}/c^\circ}{\left(c^F_{Br_2}\right)^2 c^F_{Br^-}/c^{\circ 3}} \quad (6)$$

where the superscript F signifies the free (e.g. uncomplexed) species and c° is the standard concentration conveniently taken as 1 mol L^{-1} to yield dimensionless constants. To avoid verbosity, all concentrations, c, later in this paper will be written without the explicit division by c°, unless stated otherwise.

3. Experimental

3.1. Electrolyte preparation and SoC definition

To simplify the description of the electrolyte composition, the SoC was defined as [7]: SoC = 0% is equivalent to 7.7 mol L^{-1} HBr and 0.0 mol L^{-1} Br_2; SoC = 100% corresponds to 3.35 mol L^{-1} of Br_2 and 1 mol L^{-1} of HBr. 23 samples of 50 mL each were prepared at ambient lab temperature (23 °C ± 1 °C), corresponding to SoC from 5% to 110% (beyond 100% to deeper investigate the two-phase region) in 5% (percentage point) steps. Total stoichiometric concentrations of species as a function of SoC are also presented in Table P.11 in the SM.

Stock hydrobromic acid (48 wt%, Alfa Aesar) and ultra pure water (conductivity 0.055 μS cm^{-1} at ambient laboratory temperature) from Purelab Ultra System (Evoqua) were measured using E4 Electronic Pipette LTS E4-10MLXLS (Mettler Toledo). Pure, liquid bromine (Merck) was weighted at a resolution of 0.1 g. HBr, water and Br_2 were mixed and left for a week to equilibrate vials with 2-phase system (SoC ≥ 90%). The presented method allowed for preparing the solutions with maximum uncertainty of ±0.45% (percentage point of SoC).

3.2. Improved OCP experiment

The cell schematic used for measuring the bromine electrode OCP with the liquid junction potential (LJP) eliminated is presented in Fig. 1A. The measurement set-up consisted of two cells termed A (potential measurement) and B (calibration of the glass electrode (GE)). In cell A, a monoprobe (not combined) glass pH electrode Z264946-1EA (Sigma-Aldrich) was immersed in the electrolyte consisting of HBr, H_2O, and Br_2. The GE was pre-conditioned and stored in a solution of 1 M HBr between the measurements. The circuit was completed by using a glassy carbon rod Sigradur G (HTW), carefully cleaned with acetone and then with ultra pure water, dried before use.

The calibration cell B consisted of the same GE, but immersed in pure HBr solution (without bromine) at the HBr concentration identical as in cell A. The reference electrode in this cell was a hydrogen electrode Hydroflex (Gaskatel). Oxygen in the liquid phase in cell B was removed by sparging with pure nitrogen saturated with water vapour for at least one hour before measurement and then continually sparged

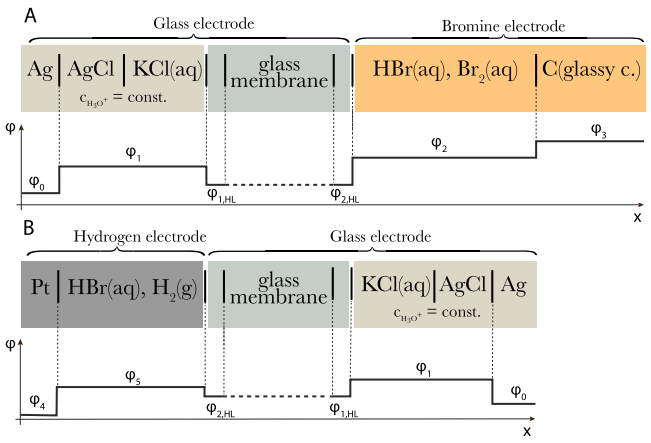

Fig. 1. A. Schematic of the proposed cell for improved OCP measurement without LJ; B. Schematic of a cell used for calibration of the glass electrode. Subscripts p in the notation of species' i activities, $a_{i,p}$, correspond to the respective regions of electric potential φ_p along spatial coordinate x.

also during the calibration step. The potential between electrodes in cell A and B was measured with an auxiliary electrometer of a potentiostat Reference 3000 (Gamry, input impedance of 100 TΩ). The cells were enclosed in a grounded Faraday's cage due to high internal impedance of the GE. Both cells A and B were thermostated at the same temperature (25 °C ± 0.1 °C or 43 °C ± 0.1 °C)

To obtain one experimental point of cell potential at given SoC, the following procedure was adopted:

1. Insert the GE into cell B, wait for a stable potential and thermal equilibrium (drift less than 0.1 mV min^{-1});
2. Record the potential of cell B (calibration);
3. Quickly transfer the GE into cell A and wait for a stable potential;
4. Record the potential of cell A (measurement);
5. Transfer the electrode back to cell B, first washing the GE from any Br_2 with a fresh portion of the electrolyte from cell B;
6. Record the potential of cell B again (re-calibration).

Next, the potential of the bromine electrode was calculated by subtraction of the arithmetic mean of potentials obtained in steps 2 and 6 from the potential obtained in step 4. If the standard deviation of the sample of the two GE calibration potentials was larger than 0.8 mV, the procedure was repeated.

OCP measurements were taken for all 23 samples at two temperatures 25 °C and 43 °C. It was found that the samples measured at 43 °C required more time to reach equilibrium (and thus stable potential), and were pre-conditioned in a thermal bath for 4 h before measurement.

Additionally, to assure that the activity of liquid water (which is a function of dissolved species) does not influence the potential in cell B, an electrode stress test was performed. Details of the stress test are provided in Appendix M in the SM.

Information of the original (primal) OCP experiment without the LJP elimination and data on experimental uncertainty calculations are presented in Appendix B and Appendix O in the SM.

3.3. Pilot-scale cell cycling with OCV pauses

The validity of the positive half cell OCP model was examined in a real-working pilot-scale HBFB single cell (geometric area of 64 cm^2). The cell was operated galvanostatically at 300 mA cm^{-2}, maintaining the electrolyte temperature at 50 °C (±5 °C inside the cell under load). Starting from the electrolyte composition of 6 mol L^{-1} HBr and 0.3 mol L^{-1} Br_2 (300 mL sample) and hydrogen side pressure at 0.6 bar

Table 1
Literature values for polybromide equilibrium constants.

Quantity	Value	Source	Remarks
K_3'	16.2	[19]	At 25 °C, distribution of Br_2 between CCl_4 and aqueous phase.
K_3'	16.0	[20]	At 25 °C, distribution of Br_2 through vapour phase, with potassium bromide as the source of Br^-.
K_3'	18.55–16.18	[29]	At 16.5–21.5 °C, using the method of [19] with different sources of bromide (HBr, KBr, NaBr, LiBr). K_3' varied with ionic strength and type of salt.
K_3'	16.73	[26]	At 25 °C, vapour partitioning method, low ionic strengths, no correction for activity coefficients.
K_3'	19.85, 16.85, 15.28	[24]	At 5, 25, 35 °C, respectively, vapour equilibration method, low ionic strengths ($I_m = 0.5$ mol kg^{-1}), and low Br_2 concentrations (mmols), no correction for activity coefficients, correction for suspected bromine hydrolysis.
K_3	14.18	[18]	Fitting an OCV model to experimental data, taking into account activity coefficients of HBr (different activity models) and Br_2
K_5'	40 and 18.2	[25]	At 0 and 25 °C, respectively
K_5'	40	[20]	At 25 °C, distribution of Br_2 through vapour phase, with potassium bromide as the source of Br^-.
K_5'	37.7	[26]	At 25 °C, vapour partitioning method, low ionic strengths, no correction for activity coefficients.
K_5'	38.51, 25.3, 19.86	[24]	At 5, 25, 35 °C, respectively, vapour equilibration method, low ionic strengths ($I_m = 0.5$ mol kg^{-1}), and low Br_2 concentrations (mmol), no correction for activity coefficients, correction for suspected bromine hydrolysis.
K_5	262.47	[18]	Fitting an OCP model to experimental data, taking into account activity coefficients of HBr (different activity models) and Br_2. The originally reported K_5 was defined as sequential formation $\beta_5^* = a_{Br_5^-}/(a_{Br^-}\, a_{Br_2})$ (See Appendix E in the SM for discussion) and its value was $K_5/K_3 = 18.51$.

gauge (no pre-humidification), the cell was charged and discharged during a test procedure. At predefined intervals, the potentiostat was switched to OCV mode for one minute to allow for potential relaxation. The OCV in equilibrium was then recorded and small electrolyte samples were collected for SoC analysis. More details on the test procedure, materials, electrolyte samples analysis method and used equipment are listed in Appendix N in the SM.

4. Mathematical modelling

4.1. Modelling of the complexes formation

The posolyte in HBFB is assumed to contain the following species:

1. Protons (hydronium cations), H_3O^+
2. Free dissolved bromine, Br_2
3. Free dissolved bromide, Br^-
4. Tribromide, Br_3^-
5. Pentabromide, Br_5^-
6. Heptabromide, Br_7^-
7. Pure liquid water (solvent), H_2O

It is assumed that the only electron transfer reaction is represented by Eq. (4). In essence, the polybromide complexes act as a "buffer" for bromide and bromine, but themselves are considered electrochemically inactive.

In a Nuclear Magnetic Resonance (NMR) study of a similar phenomenon of triiodide formation [30], it was concluded that an exchange of iodine between free and complexed forms takes place much more rapidly than the diffusion-controlled reaction limit and these equilibrium reactions are considered as one of the fastest known in nature. As an additional support of this hypothesis, a Raman spectroscopy peak at high SoC can be assigned to vibrations of free bromine, as opposed to other coexisting peaks stemming from polybromides [7].

4.1.1. Formation of heptabromides

According to a recent study using Raman spectroscopy [7], formation of higher polybromides (most probably heptabromide) is hypothesised at high bromine concentrations:

$$3Br_2 + Br^- \overset{K_7}{\rightleftharpoons} Br_7^- \tag{7}$$

The stoichiometric equilibrium constant for reaction (7) is:

$$K_7' = \frac{c_{Br_7^-}}{\left(c^F_{Br_2}\right)^3 c^F_{Br^-}} \tag{8}$$

4.1.2. True thermodynamic constants

True thermodynamic properties are commonly described with the use of the concept of activities, a_i, which are defined as

$$a_i = \gamma_i c_i / c_i^\circ \tag{9}$$

where γ_i is the activity coefficient based on the molar concentration.[1] In order to express the ionic equilibria (Eqs. (5), (6) and (8)) in a thermodynamically consistent way, concentrations must be replaced by ionic activities, for instance:

$$K_3 = \frac{a_{Br_3^-}}{a^F_{Br_2}\, a^F_{Br^-}} \tag{10}$$

Using Eq. (9), the quotient can be rewritten as

$$K_3 = \frac{c_{Br_3^-}}{c_{Br_2} c_{Br^-}} \frac{\gamma_{Br_3^-}}{\gamma_{Br_2}\gamma_{Br^-}} \tag{11}$$

or, equivalently, introducing the non-ideality term, $\Gamma_s(c,T)$, enclosing activity coefficients :

$$K_3(T) = K_3'(c,T)\Gamma_3(c,T) \tag{12}$$

The equilibrium constants defined in this way should be dependent solely on temperature. A major theoretical issue that has dominated the literature concerning these equilibria is the correction for the solution activity, here expressed as $\Gamma_s(c,T)$. Ideally, knowing γ of all species in Γ_s would be desired. It is, however, not possible to determine activities of individual ionic species, and accessing activities of uncharged species in mixtures is intricate. A detailed discussion on this topic and assumptions can be found in Appendix G in the SM.

4.2. Mass balances at equilibrium

This section derives material balances necessary to calculate electrolyte speciation.

In the bulk solution, the electroneutrality must hold:

$$\sum_i z_i c_i = 0 \tag{13}$$

which provides the first governing equation for the considered system, valid for each SoC step:

$$c^F_{Br^-} + c_{Br_3^-} + c_{Br_5^-} + c_{Br_7^-} = c_{H_3O^+} \tag{14}$$

Next, it is convenient to group the dissolved bromine concentrations together by writing:

$$c^F_{Br_2} + c_{Br_3^-} + 2c_{Br_5^-} + 3c_{Br_7^-} = c_B \tag{15}$$

[1] Please note that throughout this paper, the molar and molal activity coefficients are denoted as γ and y, respectively.

where c_B is the total molar concentration of bromine-containing species. Finally, from equilibrium relationships (5), (6), and (8), three additional equations can be formulated:

$$K_3' \; c_{Br_2}^{F} \; c_{Br^-}^{F} = c_{Br_3^-} \tag{16}$$

$$K_5' \; c_{Br_2}^{F\;2} \; c_{Br^-}^{F} = c_{Br_5^-} \tag{17}$$

$$K_7' \; c_{Br_2}^{F\;3} \; c_{Br^-}^{F} = c_{Br_7^-} \tag{18}$$

Eqs. (14)–(18) present a system of equations which admit an analytical solution, where the unknowns are the equilibrium concentrations $c_{Br^-}^{F}$, $c_{Br_3^-}$, $c_{Br_5^-}$, $c_{Br_7^-}$ and $c_{Br_2}^{F}$. The concentrations prior to equilibrium $c_{H_3O^+}$ and c_B are provided as parameters dependent on the desired SoC. Solution details are available in Appendix F in the SM. Accordingly, the remaining equilibrium concentrations are computed from Eq. (14).

It follows from the hypotheses presented in Appendix G in the SM that $\Gamma_s = 1$ and K_s' are equivalent to K_s and will be designated herein as the latter. A discussion on the consequences and practical validity of such treatment is presented in Section 5. Finally, to model the OCP, the calculated values of $c_{Br^-}^{F}$ and $c_{Br_2}^{F}$ were used in Eq. (19) together with activity coefficients. The details on computation of activity coefficient and posolyte density are provided in Appendix J and Appendix K in the SM.

4.3. Computation of equilibrium constants from the improved OCP experiment

The whole GE half-cell acts as a pseudo-reference electrode for the glassy carbon electrode while avoiding the build-up of the liquid-junction potential always present when utilising ordinary reference electrodes. The GE half-cell reference potential is established by the double calibration in cell B, assuming that the presence of uncharged bromine does not influence the activity of water in the hydrated layer of the glass membrane. The potential of cell A referenced against a hypothetical reversible hydrogen electrode (RHE) immersed in the same solution can be described using the following equation (refer to Appendix C in the SM for details regarding the derivation thereof and to Appendix H for the meaning of mean activity coefficients used here):

$$E_{OCP} = E^{\circ}_{Br_2/Br^-} - \frac{RT}{F} \ln \frac{c_{Br^-}^{F} c_{HBr}^{T} \gamma_{HBr}^{\pm\;2}}{\sqrt{c_{Br_2}^{F}}} \tag{19}$$

where the superscript T signifies the total species concentrations. Rearranging Eq. (19) to obtain the ratios, r, of free electrode-active species concentrations yields:

$$r = f(E_{OCP}, c_{HBr}^{T}) = \frac{c_{Br^-}^{F}}{\sqrt{c_{Br_2}^{F}}} = \frac{\exp\left[F(E^{\circ}_{Br_2/Br^-} - E_{OCP})/(RT)\right]}{c_{HBr}^{T} \gamma_{HBr}^{\pm\;2}} \tag{20}$$

$\gamma_{HBr}^{\pm}$ is modelled using a method described in Appendix J in the SM, E_{cell} is measured and $E^{\circ}_{Br_2/Br^-}$ is given by Eq. (L.11) in the SM. $\gamma_{HBr}^{\pm}$ is always evaluated at c_{HBr}^{T} i.e., at an ionic strength equal to c_{HBr}^{T}, considering that the electrostatic contributions of Br^-, Br_3^-, Br_5^-, and Br_7^- to the ionic atmosphere are indistinguishable.

All the bromine species obey mass balance, therefore:

$$c_{Br_2}^{C} = c_{Br_2}^{T} - c_{Br_2}^{F} \tag{21}$$

$$c_{Br^-}^{F} = c_{Br^-}^{T} - c_{Br^-}^{C} \tag{22}$$

where the superscript C is used to refer to the overall concentration of complexed species.

Raman spectra of the electrolyte available in [7], provided the information on relative amounts of bromine in each polybromide species s, x_s, as depicted in Fig. R.13 in the SM. Equivalently, x_s is the fraction of the whole complexed bromine, $c_{Br_2}^{C}$, contained in polybromide s. Thus, dividing each x_s by the stoichiometric coefficient of Br_2 present in each of the polybromides (e.g. there are three moles of Br_2 per one mole of Br_7^-), it is possible to calculate the concentration of the total complexed bromine as:

$$c_{Br^-}^{C} = c_{Br_2}^{C}(x_{Br_3^-} + x_{Br_5^-}/2 + x_{Br_7^-}/3) \tag{23}$$

For each SoC step, gathering the terms in parentheses, the above equation can also be written shorter as:

$$c_{Br^-}^{C} = c_{Br_2}^{C} X \tag{24}$$

Substitution of Eqs. (21) and (22) to (24) yields:

$$c_{Br^-}^{F} = c_{Br^-}^{T} - (c_{Br_2}^{T} - c_{Br_2}^{F})X \tag{25}$$

From Eq. (20), the free bromine concentration is calculated as:

$$c_{Br_2}^{F} = \left(c_{Br^-}^{F}/r\right)^2 \tag{26}$$

with $c_{Br^-}^{T} = c_{HBr}^{T}$.

Replacing $c_{Br^-}^{F}$ in Eq. (26) with Eq. (25), solving analytically for $c_{Br_2}^{F}$, and choosing only the non-negative and real solution yields:

$$c_{Br_2}^{F} = \Big(-r\sqrt{r^2 + 4X^2 c_{Br_2}^{T} - 4X c_{HBr}^{T}} + r^2 + 2X^2 c_{Br_2}^{T} - 2X c_{HBr}^{T} \Big) / (2X^2) \tag{27}$$

where r is equal to the ratios calculated using Eq. (20) at given SoC. The respective equilibrium constants can now be calculated as:

$$K_s = \frac{c_{Br_2}^{C} x_s / [(s-1)/2]}{c_{Br^-}^{F} \left(c_{Br_2}^{F}\right)^{(s-1)/2}} \tag{28}$$

where $s \in \{3, 5, 7\}$. The formation constants computed here are based on molar concentrations.

4.4. Modelling of the full HBFB cell OCV

The described versatile bromine side model is flexible to address any physical definition of the SoC, because the model input consists of molar concentrations of species rather than the SoC defined arbitrarily and *ad hoc* for an RFB system. In order to compare the improved model to a real HBFB, an expression for the negative half cell is necessary. In the literature [14–17,31,32], the common Nernst equation for the hydrogen half cell is in the form:

$$E_{eq,H^+/H_2} = E^{\circ}_{H^+/H_2} + \frac{RT}{2F} \ln \frac{a_{H^+}^2}{a_{H_2}} \tag{29}$$

The problem of single-ion (proton) activity is circumvented by writing out the equation for cell OCV and making use of Eqs. (9) and (B.7) in the SM:

$$E_{OCV} = E_{eq,Br_2/Br^-} - E_{eq,H^+/H_2} = E^{\circ}_{Br_2/Br^-} + \frac{RT}{2F} \ln \frac{a_{Br_2}^{F} a_{H_2}}{\left(c_{H^+}/c^{\circ}_{H^+} c_{Br^-}^{F}/c^{\circ}_{Br^-}\right)^2 \gamma_{HBr}^{\pm\;4}} \tag{30}$$

It is vital to note that for e.g. proton-exchange membrane fuel cells, the term c_{H^+} normally vanishes due to its equal contribution to the half-cell OCP on both sides. In hybrid RFBs such as HBFB, however, protons are not consumed electrochemically in the positive half cell. It is customary [14] to take the proton concentration as the concentration of fixed sulphonic groups in the membrane, which depends on the membrane equivalent weight. In this model, a value of $c_{H^+} = 1000\ \mathrm{mol\,m^{-3}}$ will be assumed, following [14,15].

The activity of free bromine is taken equal to the calculated free concentration due to reasons discussed in detail in Appendix G. The

concentration of free bromide is calculated using equations presented in Section 4.2. $\gamma^{\pm}_{HBr}$ is always evaluated at known c^{T}_{HBr}. The activity of hydrogen gas due to its moderately low pressure in a typical HBFB (max. tens of bars absolute pressure) is modelled by $a_{H_2} = p_{H_2}/p°$ where p_{H_2} is the average partial pressure of hydrogen gas in the negative half cell compartment and $p°$ is the standard pressure equal to 1 bar. Due to uncertainty of assumption whether the dry hydrogen fed to the cell became saturated with water vapour or not, two modelling cases were investigated. In the first case, it was assumed that the hydrogen is fully saturated with water vapour at the operating temperature of 50°C, hence $p_{H_2} = P - p_{H_2O}$, where P is the mean total pressure in the half cell and $p_{H_2O} = 0.124$ bar is the water vapour saturation pressure [33]. In the second case, hydrogen was assumed dry, hence $p_{H_2} = P$. For reference, the cell OCV was also modelled using simple Nernst equation akin to the common modelling approach.

4.5. Concentration polarisation

Another aspect of the thermodynamic analysis of RFB operation is a phenomenon induced by a finite rate of mass transport to the electrode. Albeit pertaining specifically to a cell under load (i.e. away from the state of thermodynamic equilibrium analysed hereto), the phenomenon termed concentration polarisation has its roots in thermodynamics and thus will be briefly discussed. The polarisation of an RFB cell under load is commonly described by a sum

$$E_{cell} = E_{OCV} - IR - \eta^{act} - \eta^{c}_{+} - \eta^{c}_{-} \tag{31}$$

where E_{cell} is the RFB cell voltage, IR is the product of cell current (positive for discharge) and all cell ohmic resistances, η^{act} is the activation polarisation of both anode and cathode (positive for discharge), and η^{c}_{+}, η^{c}_{-} are the concentration polarisations of the positive and the negative half cells, respectively.

When a cell is driven out of equilibrium and the current is flowing, the concentration of a reactant at the electrode surface (e.g. carbon fibres) differs form the one in the bulk, thus creating a local difference in electrochemical potentials, which in turn translate to electric potential build-up. The most common way to thermodynamically describe η^{c} is to consider a Nernst-type equation [34]. Moreover, there normally exists only one (limiting) reactant which contributes most significantly to the concentration polarisation. Since in HBFB, compared to gaseous hydrogen side, the liquid bromine side is the limiting half cell [16], for the purpose of this analysis it is reasonable to set $\eta^{c}_{+} \gg \eta^{c}_{-}$. Furthermore, the diffusion coefficient of bromine in water is roughly 80% of the one of bromide [16], hence it is rational to focus the concentration polarisation analysis on the process involving bromine as reactant (discharge).

Following the derivation from for example [34], η^{c} on HBFB discharge can be described by

$$\eta^{c} \approx \eta^{c}_{+} = \frac{RT}{nF} \ln\left(1 - i/i_{lim}\right) \tag{32}$$

where i is the cell current density and i_L is the limiting current density at given bulk electrolyte composition. It is evident that Eq. (32) does not include any reaction kinetic parameters as it was derived from thermodynamics. The magnitude of η^{c} with respect to cell OCV at given i_L was analysed in Section 5.4 both theoretically and in a cell overpotential breakdown.

4.6. Adopted analysis approach

This sub-section provides a summary of performed systematic analyses (Studies), whose results are presented in Section 5.

In Study 1, the purpose was to analyse the modelled OCP curves and species concentration distributions assuming the literature values for tri- and pentabromide formation constants. A paper of Ramette and Palmer [26] was selected as a reliable source of formation constant values ($K'_3 = 16.72$ and $K'_5 = 37.7$ at 25 °C) as it contains a short review of precedent studies and additional experimental investigations. Both values were plugged into the OCP model described in Section 4 with no heptabromide formation assumed ($K'_7 = 0$). The OCP curves were compared with the improved OCP experiment and conclusions on species distribution over the SoC range were drawn.

Next, in Study 2, the new formation constants K_3, K_5, and K_7 were determined. The constants were plugged into the OCP model (Section 4) and the results on the predicted potential and speciation across the SoC range were analysed. This study was conveyed for 25 °C, and repeated for 43 °C, using the experimental data on the OCP at 43 °C and assuming that the relative amounts of bromine in polybromides (x-values) obtained from Raman spectra remain constant in the considered temperature range. The Raman spectra were not available for temperature other than 23 °C ± 1 °C, hence the assumption.

In Study 3, the validated OCP model was used to create a 3D-plot of the OCP vs. RHE for a given total concentration space of bromine and bromide species. Finally, the bromine electrode OCP was combined with the hydrogen electrode OCP description to yield an expression for the full cell OCV. The OCV model was then validated against experimental data. The thermodynamic η^{c} was compared with a full cell model by Huskinson et al. [16].

5. Results and discussion

5.1. OCP experiments

The results of the OCP measurements are presented in Fig. 2. Tabular data with the results of the improved OCP experiment is also available in Table P.11 in the SM. Note that at certain concentration combination (at SoC 90% in this case), bromine reaches saturation in water and HBr mixture and separates into a two-phase system. The two curves from the improved OCP experiment at 25 °C and 43 °C are compared with that from the original OCP experiment. The potential calculated with the simple Nernst equation, Eq. (33), is superimposed for reference. The input to the Nernst equation was c^{T}_{HBr} and $c^{T}_{Br_2}$, following the SoC definition.

It is vital to distinguish the reference potential with respect to which the presented curves are reported. The improved OCP experiment data is reported versus RHE, i.e. the hydrogen electrode immersed in the same electrolyte as the investigated bromine electrode (herein by bridging the two electrodes with the GE to avoid reaction of bromine with platinum alloy and the build-up of the LJP). The original OCP experiment results are reported vs. SHE by converting the measured potentials using the known value of the Ag/AgCl reference electrode potential.

By adding a term $(RT/F)\ln(c^{T}_{Br^-}\gamma_{Br^-})$ (the hydrogen pressure at ambient laboratory conditions assumed close to the standard pressure of 1 bar) to the experimental data of the improved OCP experiment at 25 °C, an attempt was made to reference the potential against the SHE. The curve is presented in Fig. 2 in light grey with markers. As soon as the cell potential is investigated in terms of separate half-cell potentials, a hypothesis on individual activity coefficients (here taken as $\gamma_{Br^-} = \gamma_{HBr}$) must be introduced because of the appearing and experimentally inaccessible individual activity coefficients. Moreover, electroneutrality condition requires that $c^{T}_{Br^-} = c_{H^+} = c^{T}_{HBr}$.

Inspection of Fig. 2 reveals important features of the bromine electrode. The OCP at elevated temperature decreased slightly with respect to the standard temperature of 25 °C. The potential varies fairly linearly until SoC 80%. Then, the slope increases, possibly due to the onset of higher polybromides formation. By and large, the electrode's OCP changes with SoC much more significantly than it would result from the predictions made with the simple Nernst equation. Comparing the curves having the same reference potential (SHE) with the Nernst equation, it is evident that the non-idealities in the concentrated system induce a prominent discrepancy of the measured potential with respect

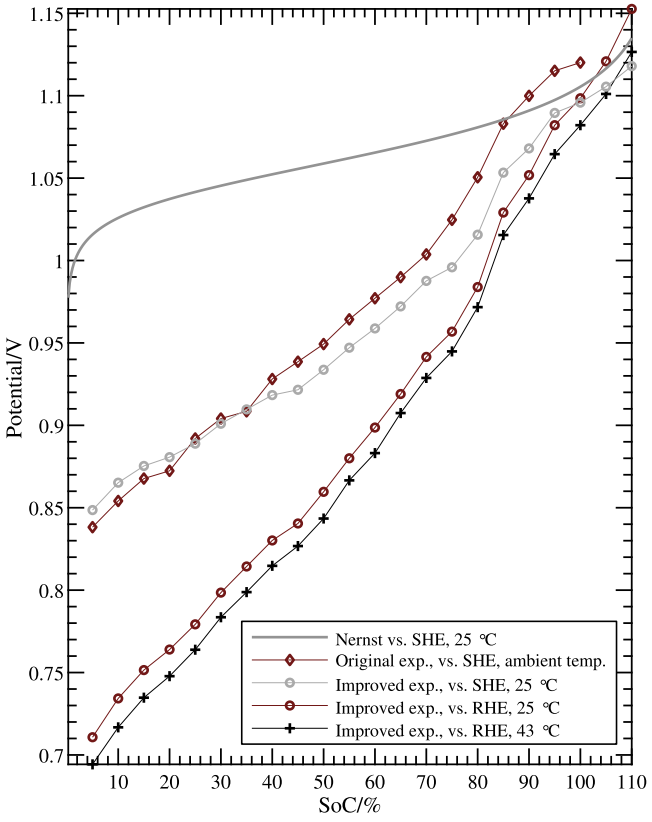

Fig. 2. Collated results from the cell potential measurements for the original OCP experiment at ambient temperature and the improved OCP experiment at 25 °C and 43 °C. Note the difference of reference potentials. The OCP scaled to SHE as well as potential calculated using the Nernst equation at 25 °C are also plotted for comparison. Error bars are of the size of the markers. The OCP measured in the improved experiment had the LJP eliminated, while the one in the original experiment — had not. Lines connecting the experimental points are shown to indicate the trend only. Please refer to Appendix O in the SM for more information about experimental uncertainty.

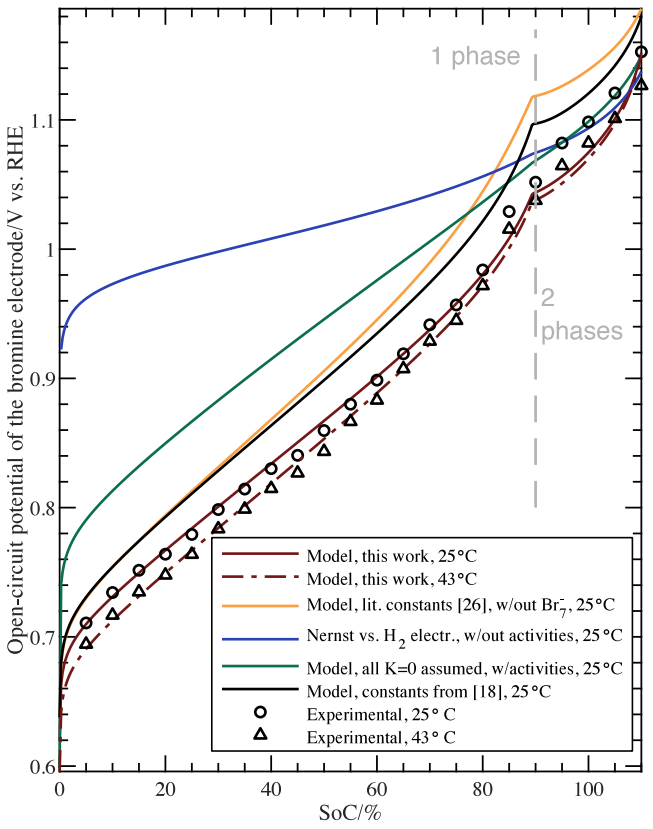

Fig. 3. OCP prediction using the presented model for different equilibria scenarios and for various model scenarios. Literature constants are $K_3' = 16.72$ and $K_5' = 37.7$ [26] or $K_3 = 14.18$ and $K_5 = 262.47$ [18]. All simulated potential curves with given equilibrium constants are reported vs. RHE. The curve referring to the Nernst equation shows the voltage between bromine and hydrogen electrodes with concentrations used instead of activities. The model without complex formation assumed, takes into account the activity of HBr. Experimental data of the improved OCP experiment (vs. RHE) is provided for reference. Phase separation line plotted for 25 °C. (For interpretation of the references to colour in this figure legend, the reader is referred to the web version of this article.)

to the simplest theory. The maximum relative error is as large as 30%.

There exists a clear discrepancy between the OCP in the original and the improved experiment referenced to SHE. The possible reasons for this are: (1) LJP existing only in the original measurement set-up, (2) the introduced hypothesis on γ_{Br^-} which allows to translate the potential to the SHE and (3) a slight difference in measurement temperatures in both experiments (the ambient lab temperature of 23 °C ± 1 °C and the set 25 °C, respectively). If one assumes that effect (1) is predominant, then it becomes apparent that the LJP cancels out close to SoC 35% and it changes sign across the SoC range. The LJP sign change is possible, as described in the literature [35].

5.2. OCP modelling

Fig. 3 shows the OCP model validation and juxtaposes various assumed modelling scenarios. First, an analysis for 25 °C is discussed. The simple Nernst equation

$$E_{\mathrm{eq,Br_2/Br^-}} = E^{\circ}_{\mathrm{Br_2/Br^-}} + \frac{RT}{2F}\ln\left(\frac{c^{\mathrm{T}}_{\mathrm{Br_2}}}{c^{\mathrm{T}\ 2}_{\mathrm{HBr}}}\right) \tag{33}$$

corresponding to a cell: bromine electrode–hydrogen electrode at standard pressure without any corrections is plotted in dark blue. It shows how poorly such an OCP treatment predicts the real cell potential, especially at high ionic strength.

Next, an OCP curve modelled with the Nernst equation, but with added activity coefficients for HBr:

$$E_{\mathrm{eq,Br_2/Br^-}} = E^{\circ}_{\mathrm{Br_2/Br^-}} + \frac{RT}{2F}\ln\left(\frac{c^{\mathrm{T}}_{\mathrm{Br_2}}}{\left(c^{\mathrm{T}}_{\mathrm{HBr}}\gamma^{\pm}_{\mathrm{HBr}}\right)^2}\right) \tag{34}$$

is plotted in dark green. The agreement in one-phase region is still poor, but improves in the two-phase region (SoC ≥ 90%).

Finally, three scenarios with polybromides formation considered are presented. The first scenario (orange curve) assumes no heptabromide formation and $K_3' = 16.72$ and $K_5' = 37.7$ are taken from [26]. The second scenario (black curve) also neglects heptabromide formation, but the constants, taken from [18], are different, especially the K_5: $K_3 = 14.18$ and $K_5 = 262.47$. With K listed in [18] for higher ionic strengths (up to 4 M HBr) the model approaches the experimental points closer than with K from [26]. Nevertheless, such a model overestimates the potential by approximately 30 mV, which is within the uncertainty due to the LJP bulid-up.

Calculation of the K used to model the OCP in this work is done by averaging the K's seen in Fig. 4b in the region of least variation (SoC ≤ 80%). The newly found constants are $\log K_3 = 1.72 \pm 0.32$, $\log K_5 = 4.58 \pm 0.24$, $\log K_7 = 5.86 \pm 0.34$ at 25 °C and $\log K_3 = 1.63 \pm 0.37$, $\log K_5 = 4.41 \pm 0.26$, $\log K_7 = 5.60 \pm 0.39$ at 43 °C. From the integrated form of van't Hoff equation, assuming $(\partial \Delta H^{\circ}_{s}/\partial T)_P \approx 0$, the standard enthalpy changes of polybromide formation were approximated to:

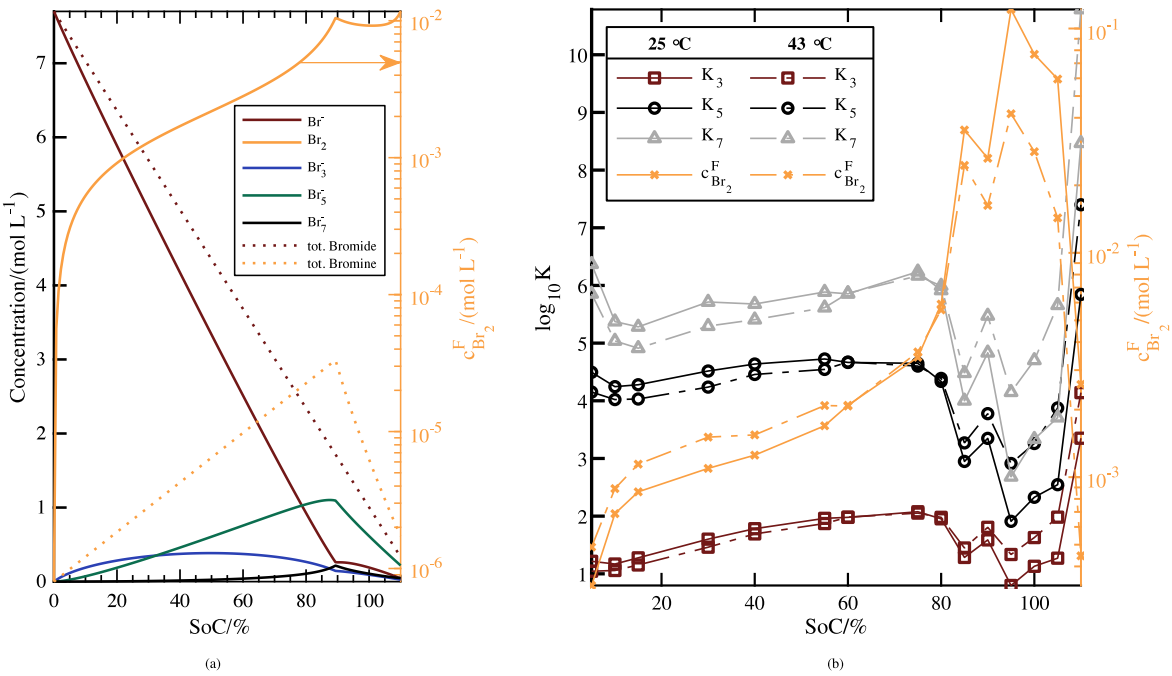

Fig. 4. (a) Species distribution in equilibrium for the base case study at 25 °C, $K_3 = 52$, $K_5 = 3.81 \times 10^4$ and $K_7 = 7.18 \times 10^5$.; (b) Polybromide equilibrium constants and free bromine concentrations calculated from the combined Raman spectra and improved OCP measurement method for 25 °C and 43 °C. Lines connecting the experimental points are shown to indicate the trend only. (For interpretation of the references to colour in this figure legend, the reader is referred to the web version of this article.)

$\Delta H_3^\circ = -8.54$ kJ mol^{-1}, $\Delta H_5^\circ = -17.07$ kJ mol^{-1}, $\Delta H_7^\circ = -25.60$ kJ mol^{-1}. These ΔH_s° agree reasonably well with [26].

Formation constants found in this study are considerably higher than the values reported in the literature to date. In the paper of Duranti et al. [18], medium concentrated solutions are used, and already much higher K_5 are calculated, which coincides with the fact that the K's measured in very diluted solutions (from older papers), are much lower than those measured at higher concentrations.

The OCP model with newly established constants (third scenario — dark red curves) predicts the potential with sufficient accuracy in the one-phase region. The observed deviation in the two-phase region is probably due to an incomplete electrode potential expression (Eq. (19)) or experimental artefacts, such as liquid bromine adhering to the glassy carbon electrode. The model also predicts well the variation of the OCP with temperature in the 1-phase region. It was found that for high bromine concentration (near saturation) and low ionic strength (below 1 M HBr), using the incomplete OCP model (Eq. (34)) yields better potential estimates.

As follows from Fig. 4a, tribromide is present in the whole SoC range, pentabromide is very abundant at higher SoC, and heptabromide is forming substantially only around the bromine saturation concentration. Free bromine concentration is much lower than the total bromine concentration (pre-equilibrium), which can be seen in both Figs. 4b and 4a. It is a support for the probable reason of invisibility of bromine in Raman spectra for low and moderate SoC.

Polybromides are difficult to quantify as they all coexist and remain in equilibrium with the uncomplexed species. Penta- and heptabromides are hard to distinguish at higher SoC because of overlapping Raman signals for both species as evidenced in Fig. R.13 in the SM and in [7].

The model was also used to explore the OCP in the bromine and bromide concentration space which is depicted in Fig. 5. It shows that at high concentration of both species within the one-phase region, the OCP varies fairly linearly, which is not the case at low concentration borders. A stand-alone application was developed and is available for both MS Windows® and MacOS®. It quickly solves the presented equations, allowing for a user-friendly OCP prediction. An installer `BromineOCP-Win.exe` or `BromineOCP-macOS.app` launching Matlab Runtime® is available online in the SM. More details are described in Appendix U in the SM.

A model of the mean activity coefficient, $\gamma^{\pm}_{HBr}$ of HBr solutions up to 11-molal based on the Pitzer framework was developed an described in Appendix J in the SM. It is capable of predicting $\gamma^{\pm}_{HBr}$ at temperatures between 0 and 70 °C, which covers the operating range of bromine-based RFBs and can be used for other modelling purposes such as developing a predictive cell performance model. In Fig. Q.12 in the SM, the mean molal activity coefficients calculated using the described model were plotted for different temperatures.

5.3. Cell OCV model validation with a pilot-scale HBFB cell

The results of the described cell cycling procedure are presented in Fig. 6 by plotting cell voltage over time. Fig. 7 shows a good agreement of the two model cases with experimental data, with a maximum relative error of −0.73%. More data is presented also in Table S.13 in Appendix S (SM). In contrast, employing the simple Nernst equation for the positive electrode, not only produces considerable error in the magnitude of OCV estimation, but also incorrectly predicts the slope of the changes. It is also concluded that while hydrogen humidity normally impacts cell performance under load, especially regarding membrane hydration, the water vapour content does not seem to significantly change the OCV values of the cell.

Even though the cell was cycled symmetrically about the cell state 4 with respect to the charge/discharge time, the influence of side reactions and species crossover through the membrane is clearly visible in the non-symmetrical OCV experimental response, which is correctly captured by the OCV model (Fig. 7), provided that the input electrolyte composition is accurately determined. It follows that by knowing the OCV, H_2 gas pressure and only one total redox species concentration (e.g. c^T_{HBr}), the concentration of the other redox species can be calculated using the provided model.

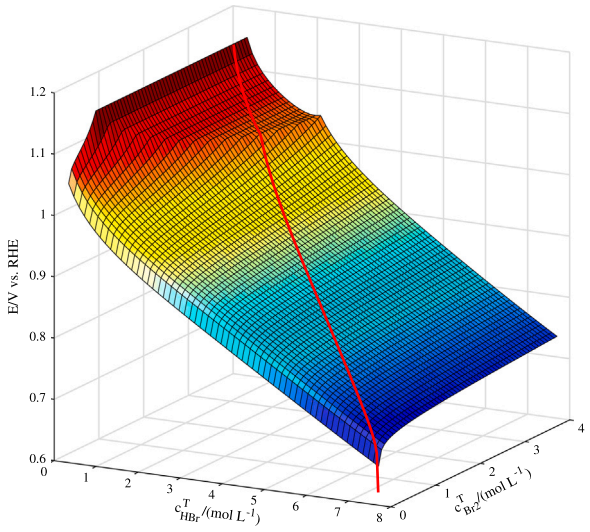

Fig. 5. 3D plot of the OCP of the bromine electrode vs. RHE at 25 °C in the electrolyte composition space. The red curve is showing the OCP variation in the composition space fixed along the adopted SoC definition. For color version of this plot, the reader is referred to the web version of this article.

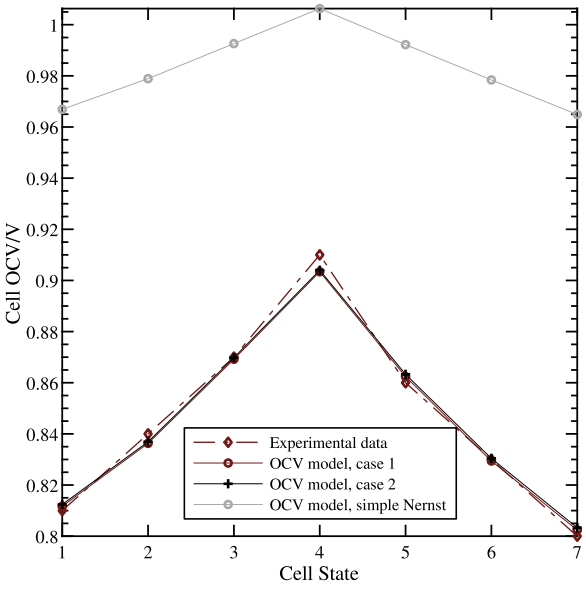

Fig. 7. Validation of the improved OCV model against experimental data. Two OCV modelling cases are presented: case 1 — hydrogen fully humidified, case 2 — dry hydrogen. Calculation of the OCV using a simple Nernst equation is given for reference. Lines connecting the data points shown to indicate trends only.

Slightly poorer agreement at cell state 4 may be associated with uncertainty of pressure measurement at the charge/discharge turnover. In general, the thermodynamic membrane potential due to different proton concentration in the membrane and in the electrolyte (assumed negligible in the OCV model) does not appear to generate excessively large errors (in theory in the range of tenths of millivolts [36]), given the large span of HBr concentrations analysed. Another source of potential error not captured by the present OCV model lies in high bromine vapour pressure at elevated temperatures. However, as evidenced by Fig. 7, this effect seems to be suppressed, because with the presence of excessive bromide anions available to form aqueous complexes, the bromine vapour pressure is dramatically reduced [7,20,24,29,37]. High partial pressure of bromine may, however, become an issue at low bromide concentrations or in electrolytes with $c^T_{Br_2}$ close to bromine solubility limit. These circumstances are, however, not the operating conditions in practical bromine-based RFB applications [16] due to economic or safety issues.

5.4. Thermodynamic concentration polarisation

Fig. 8a shows a plot of a simulated thermodynamic concentration overpotential using Eq. (32) (for $T = 323.15$ K and $n = 2$) and expressed as percentage of a typical HBFB OCV of 1.00 V. Depending on the actual mass transport conditions in the positive porous electrode and the varying battery SoC, the cell may attain a broad range of limiting currents. For the quantitative analysis, a range of typical i_{lim} between 300 and 4000 mA cm^{-2} was illustrated and for each η^c_+ was calculated. It is clear that η^c_+ increases sharply when i approaches i_{lim}. However, as evidenced in [16,38], practical RFBs never operate at current densities close to i_{lim} due to excessive ohmic heating and poor voltage efficiencies. In fact, to maintain voltaic efficiencies sufficiently high (>80%) the practical i should be much less than the i of the power density peak, which means that the cell should operate at maximum of 30%–40% of the i_{lim}. It may be therefore concluded from Fig. 8a that in typical RFB operating conditions, concentration polarisation losses due to thermodynamics solely do not outreach 1%–2% of the cell OCV. In the HBFB, the associated loss of voltage amounts to 10–15 mV. The situation may change, however, if a cell is operated (e.g. discharged) galvanostatically for a long period of time. The slowly diminishing bulk concentration of the limiting reactant will eventually drive i_{lim} to the set discharge i, and the concentration overpotential will rise rapidly.

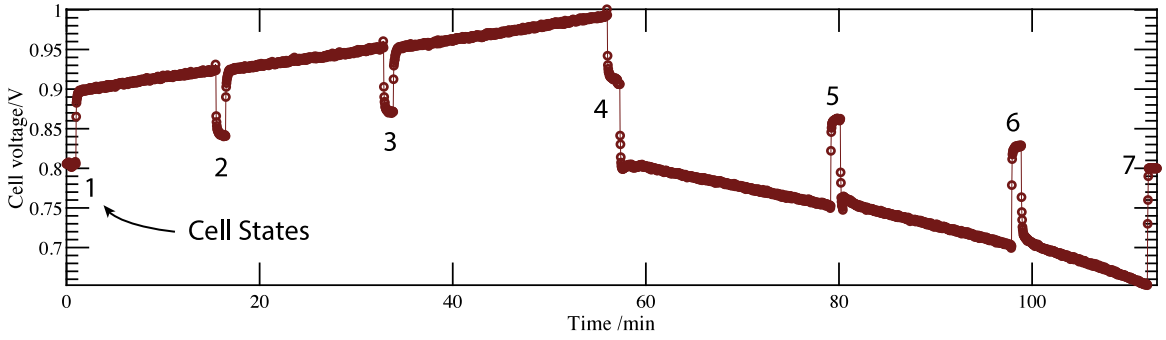

Fig. 6. HBFB single cell (64 cm^2 geometric area) galvanostatic (300 mA cm^{-2}) cycling experiment results with OCV pauses which correspond to the analysed seven cell states. States 1–3 is the charging process, 5–7 the discharging process and 4 is the charge/discharge turnover.

After subtracting ohmic, activation and thermodynamic concentration polarisation from a cell OCV, the resulting voltage corresponds to the maximum voltage of the cell, if the influence of surface concentration on electrode kinetics is neglected. In reality, however, kinetics are also affected by the depletion of the reactants in the diffusion layer close to electrode surface [34]. This effect is termed as the kinetic concentration polarisation. To scrutinise the difference between thermodynamic and kinetic η^c without resorting to the full cell model with kinetics and mass transport, the results of an advanced and experimentally validated HBFB model provided by Huskinson and al. [16] were used to obtain a typical polarisation curve with an overpotential breakdown. The analysis results are depicted in Fig. 8b.

By knowing the cell i_{lim} and T, the η_+^c was calculated from Eq. (32) and subtracted from the grey curve in Fig. 8b which represents cell polarisation without mass transport losses. The result is represented by black circles. It was found that indeed concentration polarisation due to thermodynamics only is smaller than the one due to kinetics. Using a least squares fit procedure, a scaled thermodynamic overpotential, $\zeta\eta_+^c$ was found by fitting ζ to match the actual polarisation curve (dashed line). It was determined that $\zeta = 4.15$ which implies that the kinetic η_+^c is ca. four times the thermodynamic η_+^c. Such proportionality is in line with equation (20) in [34].

The presented analysis showed that while thermodynamic concentration overpotential does not contribute significantly to cell polarisation at the operating i of RFBs, it becomes relevant at cell stress conditions or in possible fluid flow stagnation regions inside the porous electrode. This relatively simple thermodynamic investigation which did not involve any kinetic parameters allowed to conclude that the actual (kinetic) concentration polarisation can be regarded as a scaled thermodynamic contribution, the scaling factor being dependent on kinetic parameters [34]. In order to fully examine these phenomena, a more detailed model of cell under load is necessary, which falls, however, outside the scope of the present thermodynamic study.

5.5. Extension of the OCV modelling approach to other RFB systems

The promising HBFB OCV modelling results shown in this section encourage to extend the discussion to other flow battery systems. Owing to the generality of the developed model, a modification or addition of thermodynamic phenomena is manageable. The first example of such extension could be modelling of the bromine electrode OCP with additives, such as recently studied bromine complexing agents (BCAs) [6]. A systematic analysis similar to the one presented could be utilised to determine bromine complex stability constants and thus to compare bromine binding strength of different BCAs. A recently published model of a bromine-based cell with the addition of capacity-boosting additives — bromates, seemed to overestimate the voltaic efficiency as evidenced by simulated polarisation curves [39]. This error might stem from too superficial treatment of the bromine half-cell thermodynamics, which predicted too high baseline OCP potentials. Finally, the model application in other new, interesting systems such as recently studied CO_2-Br RFB [40] is feasible.

To date, the most commercial bromine-based system is the Zn–Br RFB. Modern literature on this system modelling is available [41–43], yet the OCV is most commonly treated by means of polynomial fitting or by using dilute solution theory and formal potentials for electrolyte solutions of $c > 1\ \mathrm{mol\,L^{-1}}$. There is a big potential for more rigorous parametrisation of such systems, but attention must be paid that the input properties of concentrated electrolyte solutions may vary quite drastically, as evidenced for example in Fig. J.10a (SM) regarding the difference in activity coefficients. Moreover, zinc species are also known to form ionic complexes. Emerging bromine technologies' development such as bromine-polysulfide, vanadium–bromine could also benefit from an improved electrolyte thermodynamic modelling.

Another class of RFB systems to which the presented formalism could be prospectively applied is hydrogen–halogen and other halogen-based RFBs. The former have been extensively reviewed [44]. In a recent review on the Zn–I RFB [45], Pei et al. indicated a tendency of iodine to form higher polyhalides, very similarly to the bromine chemistry, which could be studied using methods presented in this paper. Additionally, interesting phenomena influencing both OCP and kinetics of the I_2/I^- upon addition of bromide could be addressed.

According to the general trend indicated in [44], halide–halogen complexes stability constants decrease in the order I > Br > Cl (with the respective literature K_3 of 630, 16 and 0.2). It may therefore be stipulated that additional thermodynamic equilibria will affect cell behaviour more for halogen-based RFB with higher atomic number of the halogen.

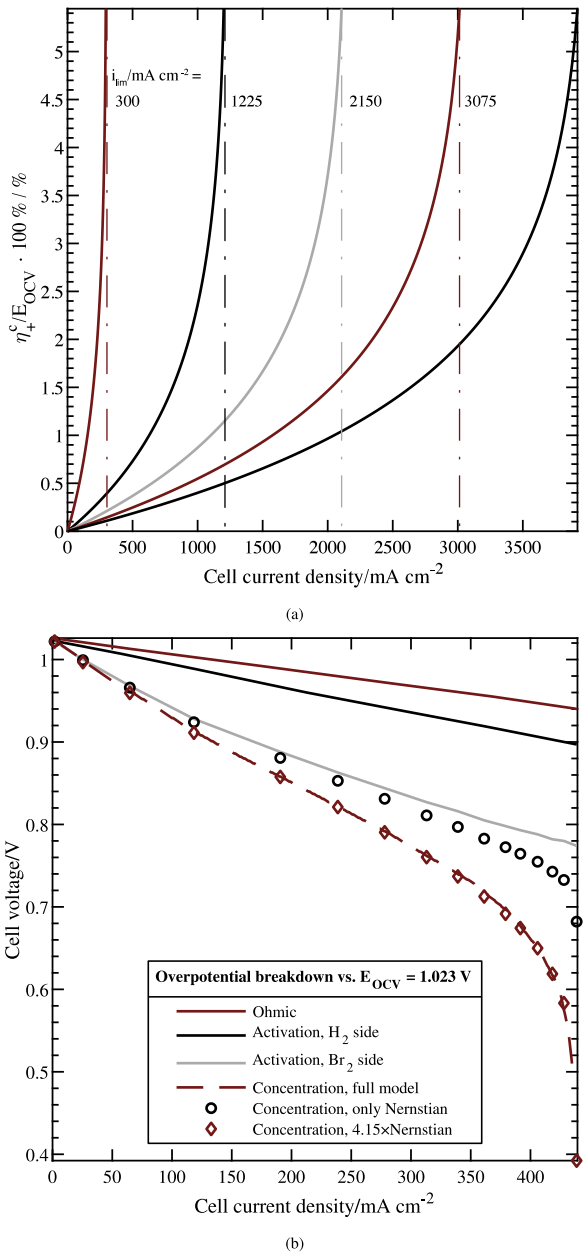

Fig. 8. (a) Thermodynamic concentration overpotential of the HBFB positive electrode on discharge (assuming Br_2 as the limiting reactant) plotted as percentage of a typical HBFB OCV of 1.00 V for five different values of i_{lim} using Eq. (32) (b) Breakdown of cell voltage losses using the data of [16] (base case at 25 °C) and modelled thermodynamic concentration overpotential. (For interpretation of the references to colour in this figure legend, the reader is referred to the web version of this article.)

Table 2
Acronyms and abbreviations.

Acronym	Explanation
BCA	Bromine Complexing Agent
DH	Debye–Hückel
GE	Glass Electrode
HBFB	hydrogen–bromine Flow Battery
HL	Haugaard Layer
LJ	Liquid Junction
LJP	Liquid Junction Potential
M	Molarity
m	Molality
NMR	Nuclear Magnetic Resonance
OCP	Open-Circuit Potential
OCV	Open-Circuit Voltage
RHE	Reversible Hydrogen Electrode
SHE	Standard Hydrogen Electrode
SoC	State of Charge
SM	Supplementary Material (online)

Table 3
List of Latin symbols.

Symbol	Explanation	Units/value
a	Activity	–
A_{in}	Coefficients in Eq. (K.1)	See text
A_ϕ	Debye–Hückel constant	–
b	Universal constant in Pitzer equation	1.2 $kg^{0.5}$ $mol^{-0.5}$
B^y, B^ϕ	Second virial coefficient (molality-based, osmotic coefficient-based)	–
c	Molar concentration	mol L^{-1}
C_t	Temperature coefficient	mV K^{-1}
C^y, C^ϕ	Third virial coefficient (molality-based, osmotic coefficient-based)	–
D^y	Fourth virial coefficient (molality-based)	–
$E_{eq,rc}$	Equilibrium potential of the redox couple rc	V
E°_{rc}	Standard potential of the redox couple rc	V
$E^\circ_{T,rc}$	Standard potential of the redox couple rc at temperature T	V
$\|e\|$	Norm of residuals of fit	See text
F	Faraday constant	96 485 C mol^{-1}
G	Molar Gibbs free energy	J mol^{-1}
$\overline{G}$	Partial molar Gibbs free energy	J mol^{-1}
$\overline{H}$	Partial molar enthalpy	J mol^{-1}
ΔH°_s	Standard molar enthalpy change of polybromide formation	kJ mol^{-1}
i	Current density	mA cm^{-2}
$\overline{J}$	Relative partial molar heat capacity of the electrolyte	J mol^{-1} K^{-1}
K	Equilibrium constant	–
k_B	Boltzmann constant	1.38065×10^{-23} J K^{-1}
$\overline{L}$	Relative partial molar enthalpy of the electrolyte	J mol^{-1}
$\overline{L^\phi}$	Relative (to infinite dilution) apparent molar enthalpy of the electrolyte	J mol^{-1} K^{-1}
m	Molal concentration	mol kg^{-1}
M_i	Molar mass of substance i	kg mol^{-1}
n	Number of electrons transferred	–
N_A	Avogadro's constant	6.0221×10^{23} mol^{-1}
n_i	Number of moles of species i	mol
Q	Term in Eq. (B.9)	V
q_e	Elementary charge	1.60218×10^{-19} C
P	Total pressure	bar
p_i	Partial pressure of gas i	bar
R	Universal gas constant	8.3145 J mol^{-1} K^{-1}
r	Ratio in Eq. (20)	–
R_i	Empirical coefficients in Eq. (K.2)	See text
r_m	Resolution of voltage measurement	V
s	Number of bromine atoms in a polybromide molecule, integer	$s \in \{3, 5, 7\}$
S	Molar entropy of reaction	J mol^{-1} K^{-1}
T	Temperature	K
t	Temperature	°C
t_i	Transport number of species i	–
V	Volume	See text
w_m	Solvent mass	kg
w_n	nth electrolyte component concentration	wt%
X	Term in Eq. (24)	–
x_s	Relative amounts of bromine in each polybromide species s	–
y	Activity coefficient (molality scale)	–
z	Valence	–

6. Conclusions and outlook

The presented thermodynamic analysis of the bromine electrode for RFB applications paves the way towards deeper understanding of the important non-ideal effects such as complex formation or ionic activity, appearing in highly-concentrated RFB electrolytes. An example of a thorough analysis is provided for one of the most common and rapidly emerging bromine-based RFBs, the hydrogen–bromine system. Rudimentary RFB parameters: the half-cell OCP and the full-cell OCV of the system were chosen to show explicitly the impact of the discerned non-ideal effects on cell thermodynamics. The attempt at advancing the missing description of the bromine half cell in equilibrium, whose lack was signalised earlier by Huskinson and Aziz [16], was accomplished. This study reveals that at higher electrolyte concentrations, K_s tend to be much higher than the values reported in literature treating diluted systems. Given the observed moderate variation of K_s across the whole SoC range in concentrated solutions (Fig. 4b), the hypotheses leading to the assumption $\Gamma_s = 1$ may need to be revised and investigated in more detail. In practical cell potential calculations, however, such model performs sufficiently well. The formation of heptabromides, whose experimental evidence was delivered by Küttinger et al. [7], may impact the OCP especially at conditions close to saturation with Br_2.

Raman shifts of the polybromides can hardly be distinguished at high SoC, as seen in Fig. R.13 in the SM. This prevents a clear distinction between penta- and heptabromide species. More research on the speciation and stoichiometry of the complexes in the Br_2-HBr-H_2O system is required in order to determine a more precise thermodynamic picture. Potentiometric methods alone only provide an insight on the gross, superimposed equilibria influencing the electrode potential.

LJP poses substantial problems in practical aqueous RFB cell potential measurements. Utilising any reference electrode of the second kind with a porous LJ may introduce an error in the order of tenths of mV in highly concentrated solutions. Should high measurement accuracy be desired, a proper elimination or reduction of the LJP is crucial.

Robustness of the utilised modelling formalism allows for applying it to a class of RFBs rather than only to the herein exemplified HBFB. New systems containing concentrated solutions of bromine, other halogens or additives could be addressed with a good chance for success in improved parametrisation.

This physics-based modelling approach avoided the use notion of formal potentials, which are valid only for specific experimental conditions. It was concluded that a proper cell performance model (RFB under load) should be, from the very beginning, built on sound thermodynamic basis as it directly influences the cell kinetics. Herein, only cells at equilibrium were treated and an extension of this study to model charge and mass transport processes in concentrated RFB electrolytes is under preparation.

The cell concentration polarisation stemming from thermodynamics was shown to introduce only minor polarisation in the practical operating current densities, but becoming much more pronounced at longer galvanostatic discharges or at cell stress conditions. In order to model the phenomena of concentration polarisation more rigorously, a detailed kinetic cell model with sufficient treatment of mass transport in concentrated electrolytes is required. A manuscript on the related topics is currently under preparation.

Failure in predicting the OCP will imply imprecise calculations of the output current density and the related error will be magnified exponentially at high fluxes. This problem is common to all flow battery systems, especially aqueous ones. By and large, it is highly improbable

Table 4
List of Greek symbols.

Symbol	Explanation	Units
α_1	Universal constant in Pitzer equation	2 $kg^{0.5}$ $mol^{-0.5}$
β_0, β_1	Pitzer coefficients	–
β_s^*	Equilibrium constant assuming sequential bromine addition	–
δ	Uncertainty of measurement	See text
Δ	Change	–
ϵ_0	Permittivity of free space	8.8542×10^{-12} F m^{-1}
ϵ_R	Relative permittivity of water	–
Γ	Non-ideality term	–
η	Overpotential	V
γ	Activity coefficient (molarity scale)	–
λ_n	Coefficient of polynomial Eq. (L.8)	See text
μ	Chemical potential	J mol^{-1}
$\overline{\mu}$	Electrochemical potential	J mol^{-1}
φ	Electric potential in given phase	V
ρ_k	Density of k-component electrolyte	kg m^{-3}
ρ_0	Density of pure solvent (water)	kg m^{-3}
σ	Standard deviation	See text

Table 5
List of superscripts.

Symbol	Explanation
$'$	Stoichiometric (apparent) quantity
$^\circ$	At standard state
$^\pm$	Mean (salt activity coefficient)
act	activation
C	Complexed species
c	concentration
EX	Excess
F	Free (uncomplexed)
T	Total

Table 6
List of subscripts.

Symbol	Explanation
0	Reference
+	Positive electrode
−	Negative electrode
i	Species i
lim	Limiting
m	Molality-scale
s	Number of bromine atoms in a polybromide molecule ($s \in 3, 5, 7$).

that a straightforward application of the simple Nernst equation in any RFB modelling will guarantee satisfactory battery model predictiveness.

CRediT authorship contribution statement

Jakub K. Wlodarczyk: Writing - original draft, Methodology, Conceptualization, Visualization, Investigation, Software. **Michael Küttinger:** Writing - review & editing, Conceptualization, Investigation. **Andreas K. Friedrich:** Writing - review & editing, Supervision. **Jürgen O. Schumacher:** Writing - review & editing, Supervision, Funding acquisition.

Declaration of competing interest

The authors declare that they have no known competing financial interests or personal relationships that could have appeared to influence the work reported in this paper.

Acknowledgements

This project has received funding from the European Union's Horizon 2020 research and innovation programme under the Maria Skłodowska-Curie Grant Agreement no. 765289.

The authors greatly acknowledge Prof. Francesco Malatesta at the University of Pisa, Italy for his input and scientific guidance concerning the GE experiment. We also recognise kind help of Dr. Peter Fischer and colleagues in the laboratory at Fraunhofer ICT and also Dr. Nataliya Roznyatovskaya for making the Gamry potentiostat available. We would like to express gratitude to those who proof-read the paper and provided valuable feedback: Diego del Olmo Diaz and Dr. Michal Pavelka from the University of Chemistry and Technology, Prague, Czech Republic. Last but not least, we highly appreciate the contribution of Elestor B.V., the Netherlands, especially Dr. Kamuran Yasadi and Dr. Johanes Hugo, regarding the data for model validation in a real HBFB cell.

Appendix A. List of symbols and abbreviations

See Tables 2–6.

Appendix B. Supplementary data

Supplementary material related to this article can be found online at https://doi.org/10.1016/j.jpowsour.2021.230202.

References

[1] M.L. Perry, A.Z. Weber, Advanced redox-flow batteries: a perspective, J. Electrochem. Soc. 163 (1) (2016) A5064–A5067, http://dx.doi.org/10.1149/2.0101601jes.
[2] H. Zhang, W. Lu, X. Li, Progress and perspectives of flow battery technologies, Electrochem. Energy Rev. 2 (3) (2019) 492–506, http://dx.doi.org/10.1007/s41918-019-00047-1.
[3] D.M. Hall, J. Grenier, T.S. Duffy, S.N. Lvov, The energy storage density of redox flow battery chemistries: a thermodynamic analysis, J. Electrochem. Soc. 167 (11) (2020) 110536, http://dx.doi.org/10.1149/1945-7111/aba4e2.
[4] R.S. Yeo, D.-T. Chin, A hydrogen-bromine cell for energy storage applications, J. Electrochem. Soc. 127 (3) (1980) 549–555, http://dx.doi.org/10.1149/1.2129710.
[5] R. Ronen, I. Atlas, M.E. Suss, Theory of flow batteries with fast homogeneous chemical reactions, J. Electrochem. Soc. 165 (16) (2018) A3820–A3827, http://dx.doi.org/10.1149/2.0251816jes.
[6] M. Küttinger, R. Brunetaud, J.K. Włodarczyk, P. Fischer, J. Tübke, Cycle behaviour of hydrogen bromine redox flow battery cells with bromine complexing agents, J. Power Sources 495 (2021) 229820, http://dx.doi.org/10.1016/j.jpowsour.2021.229820.
[7] M. Küttinger, J.K. Wlodarczyk, D. Daubner, P. Fischer, J. Tübke, High energy density electrolytes for H2/Br2 redox flow batteries, their polybromide composition and influence on battery cycling limits, RSC Adv. 11 (9) (2021) 5218–5229, http://dx.doi.org/10.1039/D0RA10721B.
[8] K.T. Cho, M.C. Tucker, A.Z. Weber, A review of hydrogen/halogen flow cells, Energy Technol. 4 (6) (2016) 655–678, http://dx.doi.org/10.1002/ente.201500449.
[9] Y.A. Hugo, W. Kout, G. Dalessi, A. Forner-Cuenca, Z. Borneman, K. Nijmeijer, Techno-economic analysis of a kilo-watt scale hydrogen-bromine flow battery system for sustainable energy storage, Processes 8 (11) (2020) 1492, http://dx.doi.org/10.3390/pr8111492.
[10] K.W. Knehr, E.C. Kumbur, Open circuit voltage of vanadium redox flow batteries: discrepancy between models and experiments, Electrochem. Commun. 13 (4) (2011) 342–345, http://dx.doi.org/10.1016/j.elecom.2011.01.020.
[11] M. Pavelka, F. Wandschneider, P. Mazur, Thermodynamic derivation of open circuit voltage in vanadium redox flow batteries, J. Power Sources 293 (2015) 400–408, http://dx.doi.org/10.1016/j.jpowsour.2015.05.049.
[12] C.A.P. Muñoz, H.H. Dewage, V. Yufit, N.P. Brandon, A unit cell model of a regenerative hydrogen-vanadium fuel cell, J. Electrochem. Soc. 164 (14) (2017) F1717–F1732, http://dx.doi.org/10.1149/2.1431714jes.
[13] M.D.R. Kok, A. Khalifa, J.T. Gostick, Multiphysics simulation of the flow battery cathode: cell architecture and electrode optimization, J. Electrochem. Soc. 163 (7) (2016) A1408–A1419, http://dx.doi.org/10.1149/2.1281607jes.
[14] V. Yarlagadda, T. Van Nguyen, A 1D mathematical model of a H2/Br2 fuel cell, J. Electrochem. Soc. 160 (6) (2013) F535–F547, http://dx.doi.org/10.1149/2.050306jes.

[15] X. You, Q. Ye, T.V. Nguyen, P. Cheng, 2-D model of a H2/Br2 flow battery with flow-through positive electrode, J. Electrochem. Soc. 163 (3) (2016) A447–A457, http://dx.doi.org/10.1149/2.0361603jes.

[16] B. Huskinson, M.J. Aziz, Performance model of a regenerative hydrogen bromine fuel cell for grid- scale energy storage, Energy Sci. Technol. (2013) 16, http://dx.doi.org/10.1149/2.030202jes.

[17] R.F. Savinell, S.D. Fritts, Theoretical performance of a hydrogen-bromine rechargeable SPE fuel cell, J. Power Sources 22 (3) (1988) 423–440, http://dx.doi.org/10.1016/0378-7753(88)80035-1.

[18] M. Duranti, E.G. Macchi, L. Crema, Equilibrium properties of a bromine-bromide electrolyte for flow batteries, J. Electrochem. Soc. 167 (10) (2020) 100523, http://dx.doi.org/10.1149/1945-7111/ab98a7.

[19] A.A. Jakowkin, Ueber die Dissociation polyhalogener Metallverbindungen in wässeriger Lösung, Z. Phys. Chem. 20U (1) (1896) http://dx.doi.org/10.1515/zpch-1896-2003.

[20] G. Jones, S. Baeckström, Equilibria in aqueous solutions of bromine and potassium bromide, J. Am. Chem. Soc. 56 (7) (1934) 1517–1523, http://dx.doi.org/10.1021/ja01322a021.

[21] PubChem, Bromine, 2019, https://pubchem.ncbi.nlm.nih.gov/compound/24408 (19 Aug 2019).

[22] E.T. Branigan, N. Halberstadt, V.A. Apkarian, Solvation dynamics through Raman spectroscopy: hydration of Br_2 and Br_3^-, and solvation of Br_2 in liquid bromine, J. Chem. Phys. 134 (17) (2011) 174503, http://dx.doi.org/10.1063/1.3583477.

[23] X. Chen, M.A. Rickard, J.W. Hull, C. Zheng, A. Leugers, P. Simoncic, Raman spectroscopic investigation of tetraethylammonium polybromides, Inorg. Chem. 49 (19) (2010) 8684–8689, http://dx.doi.org/10.1021/ic100869r.

[24] D. B. Scaife, H. J. V. Tyrrell, 71.equilibrium constants for the reaction between bromine and bromide ions at 5C, 25C, and 35C in aqueous medium of constant ionic strength and acidity, J. Chem. Soc. (Resumed) (1958) http://dx.doi.org/10.1039/jr9580000386.

[25] H.A. Liebhafsky, The equilibrium constant of the bromine hydrolysis and its variation with temperature, J. Am. Chem. Soc. 56 (7) (1934) 1500–1505, http://dx.doi.org/10.1021/ja01322a016.

[26] R.W. Ramette, D.A. Palmer, Thermodynamics of tri- and pentabromide anions in aqueous solution, J. Solut. Chem. 15 (5) (1986) 387–395, http://dx.doi.org/10.1007/BF00646261.

[27] R.F.F. Savinell, Theoretical and Experimental Flow Cell Studies of a Hydrogen-Bromine Fuel Cell, Part 1. M.S. Thesis. Final Report (Ph.D. thesis), 1986.

[28] A.T. Hutton, P.W. Linder, Stability constants & their determination based in part on the article stability constants & their determination by harry m. n. h. irving which appeared in the encyclopedia of inorganic chemistry, first edition., in: Encyclopedia of Inorganic and Bioinorganic Chemistry, American Cancer Society, 2011, http://dx.doi.org/10.1002/9781119951438.eibc0210.

[29] R.O. Griffith, A. McKeown, A.G. Winn, The bromine-bromide-tribromide equilibrium, Trans. Faraday Soc. 28 (1932) 101–107, http://dx.doi.org/10.1039/TF9322800101.

[30] B. Lindman, S. Forsén, Chlorine, Bromine and Iodine N.M.R.: Physico-Chemical and Biological Applications, Softcover reprint of the original 1st ed. 1976, Springer-Verlag, Berlin, Heidelberg, 1976.

[31] H. Kreutzer, V. Yarlagadda, T.V. Nguyen, Performance evaluation of a regenerative hydrogen-bromine fuel cell, J. Electrochem. Soc. 159 (7) (2012) F331–F337, http://dx.doi.org/10.1149/2.086207jes.

[32] M.A. Vorotyntsev, A.E. Antipov, Y.V. Tolmachev, One-dimensional model of steady-state discharge process in hydrogen-bromate flow battery, Electrochim. Acta 222 (2016) 1555–1561, http://dx.doi.org/10.1016/j.electacta.2016.11.138.

[33] Water - saturation pressure, 2021, https://www.engineeringtoolbox.com/water-vapor-saturation-pressure-d_599.html?vA=50&units=C# (28 Apr 2021).

[34] B. Bosio, Concentration polarisation in heterogeneous electrochemical reactions: A consistent kinetic evaluation and its application to molten carbonate fuel cells, J. Power Sources 115 (2) (2003) 189–193, http://dx.doi.org/10.1016/S0378-7753(02)00729-2.

[35] F. Malatesta, Activity coefficients of ions in sodium halide solutions: critical remarks, Fluid Phase Equilib. 295 (2) (2010) 244–248, http://dx.doi.org/10.1016/j.fluid.2010.05.021.

[36] H.W. Harper, Calculation of liquid junction potentials, J. Phys. Chem. 89 (9) (1985) 1659–1664, http://dx.doi.org/10.1021/j100255a022.

[37] G. Jones, S. Baeckström, The standard potential of the bromine electrode, J. Am. Chem. Soc. 56 (7) (1934) 1524–1528, http://dx.doi.org/10.1021/ja01322a022.

[38] L.F. Arenas, C. Ponce de León, F.C. Walsh, Engineering aspects of the design, construction and performance of modular redox flow batteries for energy storage, J. Energy Storage 11 (2017) 119–153, http://dx.doi.org/10.1016/j.est.2017.02.007.

[39] M.F. Chinannai, H. Ju, Analysis of performance improvement of hydrogen/bromine flow batteries by using bromate electrolyte, Int. J. Hydrogen Energy (2021) http://dx.doi.org/10.1016/j.ijhydene.2021.02.149.

[40] P. Hosseini-Benhangi, C.C. Gyenge, E.L. Gyenge, The carbon dioxide redox flow battery: bifunctional CO2 reduction/formate oxidation electrocatalysis on binary and ternary catalysts, J. Power Sources 495 (2021) 229752, http://dx.doi.org/10.1016/j.jpowsour.2021.229752.

[41] B. Koo, D. Lee, J. Yi, C.B. Shin, D.J. Kim, E.M. Choi, T.H. Kang, Modeling the performance of a Zinc/bromine flow battery, Energies 12 (6) (2019) 1159, http://dx.doi.org/10.3390/en12061159.

[42] E. Manla, A. Nasiri, C.H. Rentel, M. Hughes, Modeling of zinc bromide energy storage for vehicular applications, IEEE Trans. Ind. Electron. 57 (2) (2010) 624–632, http://dx.doi.org/10.1109/TIE.2009.2030765.

[43] Z. Xu, J. Wang, S.C. Yan, Q. Fan, P.D. Lund, Modeling of zinc bromine redox flow battery with application to channel design, J. Power Sources 450 (2020) 227436, http://dx.doi.org/10.1016/j.jpowsour.2019.227436.

[44] Y.V. Tolmachev, Hydrogen-halogen electrochemical cells: A review of applications and technologies, Russ. J. Electrochem. 50 (4) (2014) 301–316, http://dx.doi.org/10.1134/S1023193513120069.

[45] Z. Pei, Z. Zhu, D. Sun, J. Cai, A. Mosallanezhad, M. Chen, G. Wang, Review of the I-/I3- redox chemistry in Zn-iodine redox flow batteries, Mater. Res. Bull. (2021) 111347, http://dx.doi.org/10.1016/j.materresbull.2021.111347.